Ab initio study of ground-state properties of the Laves phase compounds $TiCr_2$, $ZrCr_2$, and $HfCr_2$

Xing-Qiu Chen,[1] W. Wolf,[2] R. Podloucky,[1] and P. Rogl[1]
[1]*Institut für Physikalische Chemie, Universität Wien, Liechtensteinstrasse 22A, A-1090 Vienna, Austria*
[2]*Materials Design s.a.r.l., 44, av. F.-A. Bartholdi, 72000 Le Mans, France*
(Received 21 November 2004; published 4 May 2005; corrected 9 May 2005)

By the application of an *ab initio* density functional approach the structural and phase stabilities, enthalpies of formation, electronic structures, and elastic properties for the isoelectronic Laves phase compounds $TiCr_2$, $ZrCr_2$, and $HfCr_2$ in the cubic C15, and hexagonal C14 and C36 structures have been investigated. In addition, for the C14 and C15 structures of $ZrCr_2$ phonon dispersions and densities of states, temperature dependent free energies, and point defect properties have been derived from *ab initio* calculations. The comparison of the density functional data to the few existing experimental results proves the validity of the *ab initio* approach. Results for $ZrCr_2$ and $ZrMn_2$ are compared in order to corroborate the structural degeneracy for $ZrMn_2$ as predicted recently.

DOI: 10.1103/PhysRevB.71.174101 PACS number(s): 71.20.Lp, 71.15.Nc, 63.20.Dj, 61.72.Ji

I. INTRODUCTION

The nonmagnetic Cr-based Laves-phase compounds $TiCr_2$, $ZrCr_2$, and $HfCr_2$ are of technological interest because of potential applications as high-temperature structural materials[1] with excellent corrosion and oxidation resistance. Furthermore, these compounds are considered as hydrogen storage materials.[2,3] It is also important to know the point defect properties because the existence of vacancies and antisite atoms may significantly affect the mechanical properties, for example improving ductility.[4] For the enthalpy of formation experimental values are available only for $TiCr_2$ revealing large discrepancies[5,6] between measured data.

In our study we consider the three most common crystal structures of Laves phases. The C15 structure is face-centered cubic with two AB_2 formula units per unit cell with space group $Fd\bar{3}m$-O_h^7, No. 227. The C14 and C36 structures are both hexagonal types with four and eight AB_2 formula units per cell, respectively. They belong to the space group $P6_3/mmc$-D_{6h}^4, No. 194. The three structure types are related to each other due to different stackings of a basic unit.[7,8]

Recently, a very peculiar structural degeneracy for $ZrMn_2$ at low temperatures was proposed[9,10] from *ab initio* calculations which so far could not be resolved by experiment. By application of the same computational procedure the present study on the Cr-based compounds, in particular $ZrCr_2$, confirms the validity of the theoretical approach and corroborates the prediction of low temperature polymorphism of $ZrMn_2$. Differently from the Mn compounds, for the Cr-based compounds high temperature polymorphism was detected. The equilibrium phase diagrams[11] Ti–Cr, Zr–Cr, and Hf–Cr reveal that the cubic C15 structure is the stable ground state structure up to temperatures close to the melting point. At high temperatures hexagonal polytypes with C14 or C36 structure were observed.

Some density functional studies have been performed regarding the elastic properties of $TiCr_2$, $ZrCr_2$, and $HfCr_2$. Anton and Schmidt[12] calculated the lattice parameters, bulk moduli and some elastic constants for the C14 and C15 structures of $TiCr_2$ and $ZrCr_2$ by using the augmented spherical wave method and also the full potential linear muffin-tin orbital method with a gradient correction for the exchange-correlation potential (FLG). Mayer *et al.*[13] reported the lattice parameters, elastic constants, and shear moduli of the C15 phases of $TiCr_2$ and $ZrCr_2$ using a variant of the linearized muffin tin orbital method (NFP). Hong and Fu[14] calculated the elastic constants at the experimental volume of $ZrCr_2$ and $HfCr_2$ with the C15 structure using the full potential linearized augmented plane-wave method within the local density approximation (LDA). Recently, Krčmar and Fu[15] calculated point defect energies for $ZrCr_2$ with the C15 structure for the experimental lattice parameter by application of the Vienna *ab initio* simulation package (VASP) with ultrasoft pseudopotentials within the generalized gradient approximation. In this paper the enthalpy of formation for $ZrCr_2$ with the C15 structure is reported.

In our study we present a systematic *ab initio* study of the enthalpies of formation, electronic structures and elastic properties of the isovalent compounds $TiCr_2$, $ZrCr_2$, and $HfCr_2$ for the C14, C15, and C36 structures. In addition, for the C14 and C15 structures of $ZrCr_2$ the phonon dispersions, phonon densities of states and free energies are computed, enabling comparison to the vibrational properties of $ZrMn_2$ for which a phonon driven structural transition from C15 to C14 at about 200 K was proposed.[9] For $ZrCr_2$, point defect energies and related quantities are derived on the basis of supercell calculations combined with a statistic mechanical model.

II. COMPUTATIONAL DETAILS

The present results were obtained using the Vienna *ab initio* simulation package (VASP) (Ref. 16) with the projector augmented wave potential (PAW) (Refs. 17 and 18) construction. An overall energy cutoff of 400 eV was chosen. For Cr the semicore $3p$ states were also included in the set of valence states, whereas for the potentials of Ti, Zr, and Hf semicore s and p states were treated as valence states. For

TABLE I. Calculated and experimental structural parameters for $TiCr_2$, $ZrCr_2$, and $HfCr_2$ with C14, C15, and C36 crystal structures. Lattice parameters a and c in Å, equilibrium volumes V_0 per formula unit in $Å^3$, and bulk moduli B in GPa. VASP: present calculation; NFP, FLG: other calculations, see text.

	Structure	a	c	V_0	B	Method
$TiCr_2$	C15	6.857		40.3	208	VASP
		6.809		39.5	201	NFP[a]
		6.910		41.2		Expt.[b]
		6.932		41.6		Expt.[c]
	C14	4.885	7.830	40.5	199	VASP
		4.789	7.806	38.8	210	FLG[d]
		4.932	8.005	42.2		Expt.[b]
		4.900	7.927	41.2		Expt.[c]
					159	Expt.[e]
	C36	4.869	15.748	40.4	199	VASP
		4.932	16.001	42.1		Expt.[b]
$ZrCr_2$	C15	7.145		45.6	182	VASP
		7.093		44.6	179	NFP[a]
		7.026		43.4	177	FLG[d]
		7.204		46.7		Expt.[f]
		7.210		46.9		Expt.[f]
					162	Expt.[g]
	C14	5.094	8.103	45.5	176	VASP
		4.970	8.022	42.9	187	FLG[d]
		5.106	8.292	46.8		Expt.[f]
	C36	5.065	16.409	45.6	180	VASP
		5.100	16.611	46.7		Expt.[h]
$HfCr_2$	C15	7.079		44.4	199	VASP
		7.160		45.9		Expt.[i]
	C14	5.046	8.095	44.6	191	VASP
		5.067	8.237	45.9		Expt.[j]
	C36	5.022	16.301	44.5	190	VASP
		5.064	16.470	45.7		Expt.[k]

[a]Reference 13.
[b]Reference 23.
[c]Reference 24.
[d]Reference 12.
[e]Reference 26.
[f]Reference 27.
[g]Reference 28.
[h]Reference 3.
[i]Reference 29.
[j]Reference 30.
[k]Reference 31.

the exchange-correlation functional the generalized gradient approximation (GGA) of Perdew and Wang[19] was applied. Brillouin-zone integrations were performed for suitably large sets of special **k** points according to Monkhorst and Pack.[20] Optimization of structural parameters (atomic positions and lattice parameters) was achieved by minimization of forces and stress tensors. For the derivation of formation energies, the total energies of antiferromagnetic bcc Cr, hcp Ti, Zr, and Hf were calculated. All free structural parameters were fully relaxed.

The *ab initio* elastic constants were derived from total energies as a function of suitably selected lattice distortions. These energies were fitted to third-order polynomials from which the elastic constants at the equilibrium structures were calculated. The phonon dispersions and densities of states for the C14 and C15 structures of $ZrCr_2$ were derived by making use of the direct method.[21,22] This approach relies on accurate forces calculated from first principles, but is otherwise independent of the actual *ab initio* method. In our study again VASP was applied for the evaluation of forces generated by a set of independent atomic displacements within the conventional C15 and rhombohedral C14 supercells.

For $ZrCr_2$, studying point defect formation energies and related quantities, supercells of 24 atoms for the C15 structure and 48 atoms for the C14 structure were constructed. Single defects such as vacancies and antisites were considered. In order to mimic the embedding of defects in the otherwise unperturbed compound the shape and volume of the

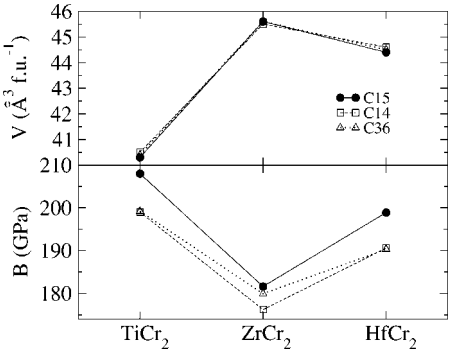

FIG. 1. *Ab initio* equilibrium volumes V_0 and bulk moduli B for the C14, C15, and C36 structures of $TiCr_2$, $ZrCr_2$, and $HfCr_2$.

supercells were kept fixed, whereas the atomic positions were allowed to relax. As reference energies for the determination of the defect formation energies the energies of formation of the compounds corresponding to the selected supercells were applied.

III. STRUCTURAL AND PHASE STABILITY

The ground state structural parameters were derived from the minimized total energies for the XCr_2 compounds with X=Ti, Zr, Hf as listed in Table I and shown in Fig. 1. In general, the volumes of the present study (line VASP) are consistently smaller by 2–3% than the experimental data. Deviations of about 4% were observed for $ZrMn_2$ (Refs. 9 and 10) for which the discrepancy was attributed to shortcomings of the local exchange-correlation approximations although GGA potentials were used. We speculate that the lattice parameters are markedly temperature dependent which in particular should affect the hexagonal structures, because they only appear at high temperatures. The results of the standard density functional calculations are, however, only strictly valid for T=0 K. Another possible reason for increased volumes might be zero point vibrations, however, due to the rather heavy masses of X=Ti, Zr, Hf, and Cr we rather expect this effect to be negligible.

The VASP volumes are significantly closer to experiment than the data of the NFP and FLG *ab initio* approaches. The smaller values obtained by NFP can be understood due to the usage of the local density approximation (LDA) rather than GGA as in our case. The more surprising are the rather small values of the FLG calculations in which GGA was applied.

According to Table I for all the compounds the hexagonal lattice parameters a for C14 and for C36 are rather similar, and they are smaller by a factor $\approx 1/\sqrt{2}$ than a for C15. For the C14 compounds the c/a ratios are close to the ideal value of $\sqrt{8/3}$, and for C36 the c/a ratio is approximately twice that of C14. The equilibrium volumes V_0 calculated by VASP for the C15 structures of $TiCr_2$ and $HfCr_2$ are smaller by about 0.1–0.2 Å^3 compared to C14 and C36, whereas for $ZrCr_2$ the trend is reversed because V_0 for the C15 structure is larger by 0.1 Å^3.

Figure 1 shows the trend of volumes and bulk moduli B revealing the largest B values for the C15 structures which are the stable ground state phases according to the total energies. One realizes the exceptional nature of the $ZrCr_2$ compound for which the volumes for all three structures are largest but the bulk moduli smallest as compared to $TiCr_2$ and $HfCr_2$. Whereas for the two latter compounds B values for the hexagonal structures are almost identical there is a significant difference between C14 and C36 for $ZrCr_2$ which is also reflected in the differences of the lattice parameters in Table I. Only two experimental results for B exist, namely for $TiCr_2$ in the C14 structure [159 GPa (Ref. 26); VASP value is 199 GPa], and for $ZrCr_2$ in the C15 structure [162 GPa (Ref. 28); VASP value is 182 GPa].[1] The difference between experiment and calculations is due to the smaller calculated volumes yielding larger bulk moduli. As discussed for the volumes, we also attribute the differences in bulk moduli to the temperature dependence of the lattice parameters and elastic properties. This holds in particular for C14 $TiCr_2$ which only exists at high temperatures. According to Table I our calculated bulk moduli are significantly smaller than the values of Anton and Schmidt[12] due to the differences in volume. These authors studied C14 $TiCr_2$ and C15 $ZrCr_2$ only. The agreement of our data to the work of Ref. 13 is much better, again because of the better agreement of the volumes as discussed. It should be noted that the pressure experiment for $TiCr_2$ (Refs. 25 and 26) was done only for the metastable C14 phase quenched to room temperature.

TABLE II. *Ab initio* enthalpies of formation ΔH in kJ mol^{-1} as compared to the available experimental data and values obtained by the application of Miedema's model (Ref. 5) for the C14, C15, and C36 structures of $TiCr_2$, $ZrCr_2$, and $HfCr_2$.

	C14	C15	C36	Miedema	Expt.
$TiCr_2$	−30.6	−35.9	−33.0	−30.3	−27.9;[a] −9.9;[b] 0.3[a]
$ZrCr_2$	−9.0	−14.5	−12.1	−51.6	
		−14.6[c]			
$HfCr_2$	−29.6	−34.9	−32.5	−29.2	

[a]Reference 5.
[b]Reference 6.
[c]Reference 15.

The calculated equilibrium enthalpies of formation with respect to the equilibrium bulk phases of the pure constituents are defined by

$$\Delta H = U_{\mathrm{DFT}}(X\mathrm{Cr}_2) - [U_{\mathrm{DFT}}(X) + 2U_{\mathrm{DFT}}(\mathrm{Cr})] \qquad (1)$$

as the difference between the corresponding total energies U of the DFT calculation, and are listed in Table II and illustrated in Fig. 2. The C15 structure is always the most stable one in accordance with the experimental findings up to rather high temperatures. The energy differences between the different structures are rather uniform with C36 being less stable than C15 by about 5 kJ mol^{-1}, and C14 is less stable than C36 by about 2–3 kJ mol^{-1}.

Currently, three experimental values for the enthalpy of formation of $TiCr_2$ are published[5,6] showing considerable discrepancies. It was not possible to find out which experimental technique was used to obtain the values −27.9 and 0.3 in Table II, the value of −9.9 kJ mol^{-1} was derived from

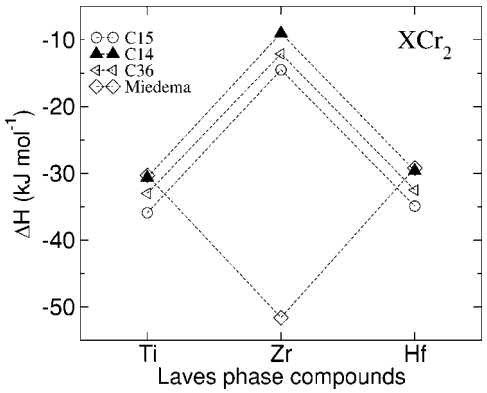

FIG. 2. *Ab initio* enthalpies of formation for $TiCr_2$, $ZrCr_2$, and $HfCr_2$ and values derived by Miedema's model.

vapor pressure measurements at temperatures from 1523 to 1653 K.[5] We believe that the experimental values are rather questionable. For $HfCr_2$ an estimation of -5.4 kJ mol^{-1} at 298 K (Ref. 5) is known. However, for both $ZrCr_2$ and $HfCr_2$ no measured values are available. As recently demonstrated for $TiMn_2$,[32] for which also calorimetric experimental data were measured, our *ab initio* approach yields reliable results for the enthalpy of formation. Furthermore, the *ab initio* value[33] of -141.2 kJ mol^{-1} for $ScAl_2$ was found to be in very good agreement to a very recent experimental value[34] of -141.6 kJ mol^{-1} obtained by reaction calorimetry, which corrected an older value[35] of -281.9 kJ mol^{-1} measured by acid solution calorimetry. Therefore, we consider the *ab initio* enthalpies of formation for the XCr_2 compounds in Table II to be reliable. In addition, the enthalpy of formation for $ZrCr_2$ of -14.5 kJ mol^{-1} agrees well with the value of -14.6 kJ mol^{-1} of another *ab initio* application.[15]

Figure 2 shows the trend of *ab initio* enthalpies of formation with $ZrCr_2$ being less stable by about a factor of 2 compared to $TiCr_2$ and $HfCr_2$. Also shown is the result obtained from Miedema's semiempirical model.[5] Although the values for $TiCr_2$ and $HfCr_2$ are in reasonable agreement with the *ab initio* data (with deviations from the values for the most stable C15 phases of about 6 kJ mol^{-1}), Miedema's model fails very badly for $ZrCr_2$ reversing the trend of the *ab initio* results. Similar failures were also found for $ZrCo_2$,[36] ZrPd, and $ZrPd_3$,[37] for which comparison was made to experimental enthalpies of formation measured by the high-temperature direct synthesis calorimetry. At least for $ZrCr_2$ we found that the bad result of Miedema's model is due to the unrealistic choice of the average density of Zr at the Wigner Seitz boundary (the parameter $n_{\mathrm{WS}}^{1/3}$ which according to conventional receipts[5] is taken to be 1.41). If a value of 1.35 would be chosen then the result of Miedema's model for the enthalpy of formation of $ZrCr_2$ is identical to the *ab initio* value. We suspect that many data derived from Miedema's model for compounds containing Zr might be corrected in the right direction by this suggestion.

Utilizing a simple model, the variation of the average electron density as expressed by the number of valence electrons per atom is correlated to cohesive properties of compounds which have a comparable type of chemical bonding. For the XCr_2 compounds the number of valence electrons are $n_X=4$ and $n_{\mathrm{Cr}}=6$ which—by application of the relation $c=(n_X+2n_{\mathrm{Cr}})/3V_0=16/3V_0$—for the C15 structures results in values of $c=0.132$, 0.117, 0.120 $e/\text{Å}^3$ for $TiCr_2$, $ZrCr_2$, and $HfCr_2$, respectively. V_0 represents the equilibrium volume as listed in Table I. Clearly, this results in the correct trend compared to the formation energies due to the opposite trend of the equilibrium volumes.

IV. ELECTRONIC STRUCTURE

In this section only the density of states (DOS) for $ZrCr_2$ is discussed because it appears to be very similar for $TiCr_2$ and $HfCr_2$. Figure 3 presents the projected local DOS (LDOS) for $ZrCr_2$ for the C14 and C15 structures in comparison to the corresponding LDOS of nonmagnetic $ZrMn_2$. The DOS for C36 is left out from the discussions because it is rather similar to C14. For all the crystal structures of $ZrCr_2$ the Fermi energy (E_F) falls into a deep minimum separating bonding and antibonding states. The value of the total DOS at E_F as expressed by the specific heat coefficient γ as listed in Table III is distinctly smallest for the C15 structure, which is the most stable structure. Our calculated value of $\gamma=4.31$ mJ mol^{-1} K^{-2} agrees well with the the experimental value[38] of 4.8 ± 0.4 mJ mol^{-1} K^{-2} by accepting a reasonable electron-phonon coupling enhancement factor of 1.12. No experimental values are reported for $TiCr_2$ and $HfCr_2$.

The LDOS clearly illustrates the *d*-*d* bonding character of the compounds. From the LDOS below E_F for both C14 and C15 structures distinct Cr-Zr hybridization features due to bonding states are identified around -1 and -3 eV, and even stronger features above E_F which build up distinct peaks at about 1, 2, and 3 eV. A well separated almost impurity-like Zr peak arises above the edge of the Cr LDOS. The features of the LDOS for the C15 structure compared to C14 are sharper and less split apart due to the higher symmetry of the cubic structure. For the C14 LDOS at -0.4 eV a distinct peak of strong Cr character arises for Cr at a (2*a*) site. This peak is missing for Cr at the (6*h*) site. Compared to (6*h*) sites the nearest neighbor distance of the Cr (2*a*) site is larger, and therefore hybridization is reduced. The same observation holds for the LDOS of nonmagnetic $ZrMn_2$ but one has to shift the energy scale by about -0.5 eV due to the larger number of valence electrons.

Now discussing $ZrMn_2$, for the nonmagnetic (NM) case (lower panels of Fig. 3) one realizes a rather rigid band behavior by shifting E_F of $ZrCr_2$ up by 0.5 eV. Then, the *d*-like LDOS (and therefore also the total DOS) is strongly increased at E_F which leads to a magnetic instability, i.e., spontaneous spin polarization occurs. For C15 the DOS at E_F is largest, and the gain in magnetic energy (i.e., the difference between the total energy of the nonmagnetic and the spinpolarized cases) is larger than for C14. For the NM $ZrMn_2$ compounds although the C14 is strongly favored by 7 kJ mol^{-1} in comparison to C15 (which is totally opposite to $ZrCr_2$) the gain in magnetic energy is just of the right magnitude in order to lead to a peculiar structural degeneracy.[9,10] Therefore, inspecting the LDOS one can attribute the unusual structural properties of $ZrMn_2$ to the states with energies between the deep minimum and E_F.

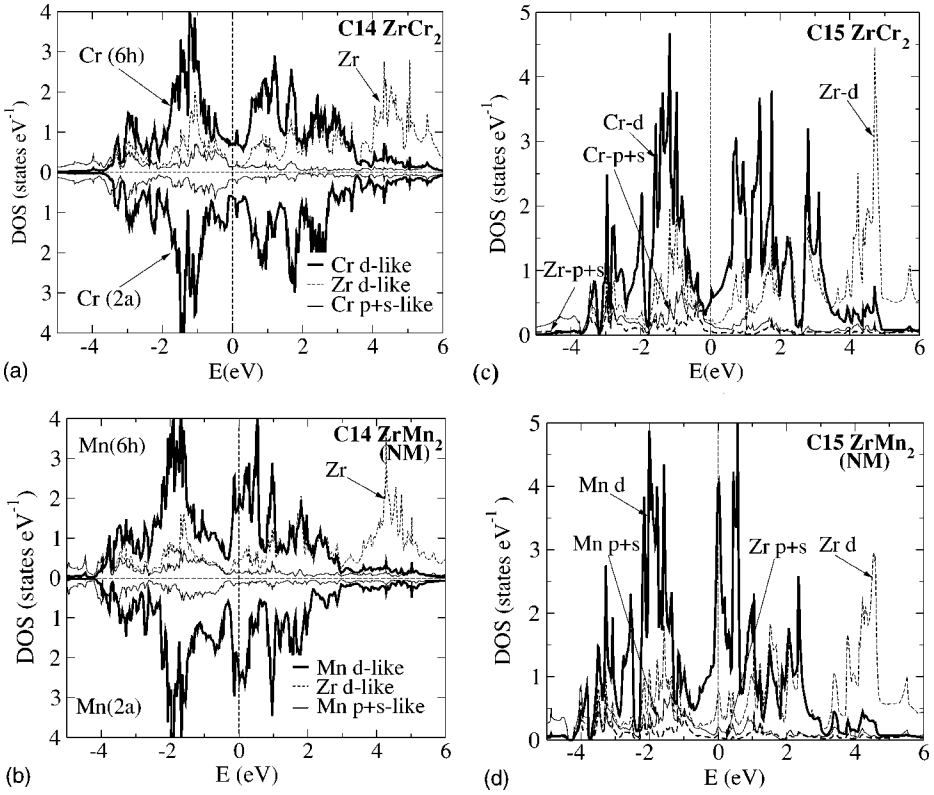

FIG. 3. Projected local density of states for the C14 and C15 structures of $ZrCr_2$ (upper panel) and nonmagnetic $ZrMn_2$ (lower panel).

On the basis of the previous discussion one might suspect that the structure dependent features of the DOS drives the relative structural stability between the compounds with C14 and C15 structures. In order to simplify the discussion, C36—which energetically lies in between C15 and C14, see Table II—is left out. Accepting this argument, we assume that the total energy difference is mainly due to the differences of band energies U_S for the structures (index S),

$$U_S(N) = \int^{E(N)} (E' - \epsilon_{F,S}) n_S(E') dE' \qquad (2)$$

denoting the total DOS by $n_S(E')$, and the structure dependent Fermi energies by $E_{F,S}$. A given energy E corresponds to the number of valence electrons by the definition $N(E) = \int^E n_S(E')dE'$. By relating the energy scales to the respective Fermi energies a common energy zero can be defined which otherwise has to be found in another way, i.e., by performing a separate tight-binding calculation for equal volumes, as done, e.g., in Ref. 39. In our case, we just considered the structure dependent DOS for $ZrCr_2$ corresponding to the respective calculated equlibrium volumes. The Fermi energies are almost equal (E_F for the C15 phase of $ZrCr_2$ is lower by 1 meV than for C14). Fine tuning of the energy reference was done in such a way that the structural energy difference $\Delta U = U_{C14} - U_{C15}$ amounts to 5 kJ mol^{-1} for $ZrCr_2$, which corresponds to the difference of total energies as listed in Table II.

Figure 4 shows the band energy difference $\Delta U(N)$ as a function of the valence electron number N. A positive value indicates that the compound with a C15 structure is predicted to be stable, a negative one that the C14 structure would be preferred. Clearly, the trend can be seen that for $ZrCr_2$ (cor-

TABLE III. Total density of states (states per eV and formula unit) and specific heat coefficient $\gamma = \frac{1}{3}\pi^2 n(E_F) k_B^2$ in mJ mol^{-1} K^{-2} at $T = 0$ K for the C14, C15, and C36 structures of of $TiCr_2$, $ZrCr_2$, and $HfCr_2$.

	C14		C15		C36	
	$n(E_F)$	γ	$n(E_F)$	γ	$n(E_F)$	γ
$TiCr_2$	1.86	4.38	1.46	3.44	1.81	4.26
$ZrCr_2$	2.09	4.92	1.83	4.31	1.93	4.54
$HfCr_2$	1.93	4.53	1.61	3.79	1.91	4.49

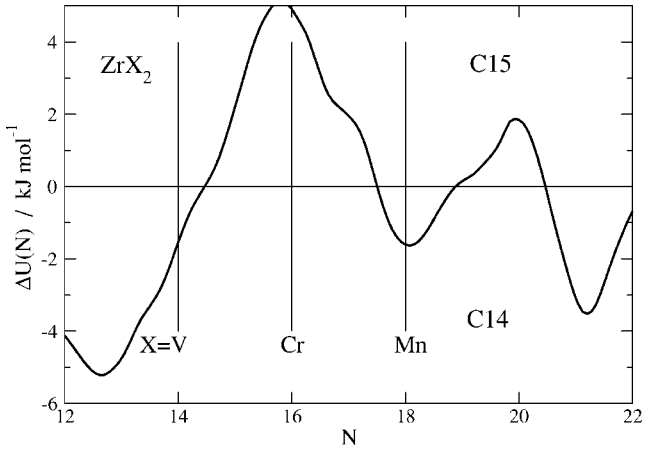

FIG. 4. Band energy difference $\Delta U = U_{C14} - U_{C15}$ as a function of valence electron number N as derived from the DOS of $ZrCr_2$.

TABLE IV. Elastic constants, bulk moduli B, and $c'=(c_{11}-c_{12})/2$ (all in GPa) at the equilibrium volumes for the cubic C15 structure of $TiCr_2$, $ZrCr_2$, and $HfCr_2$. The values for (B) are derived from volume derivatives of the volume dependent total energies.

	c_{11}	c_{12}	c_{44}	B(B)	c'	Method
$TiCr_2$	292	158	80	203 (208)	67	VASP
	322	140	99	201	91	NFP[a]
$ZrCr_2$	252	146	54	181 (182)	53	VASP
	255	141	58	179	57	NFP[a]
	201	126	46	151	38	FLAPW[b]
				162		expt.[b]
$HfCr_2$	282	152	66	195 (199)	65	VASP
	225	126	58	159	50	FLAPW[b]

[a]Reference 13.
[b]Reference 14.
[c]Reference 28.

responding to $N=16$) the C15 structure reaches its maximum stability whereas for $N=14(ZrV_2)$ and $N=18(ZrMn_2)$ the C14 structure is becoming more favorable. The total energy results for nonmagnetic $ZrMn_2$—as already discussed—indicate a strong stabilization of C14, whereas for ZrV_2 we obtain almost a structural degeneracy between C14 and C15. Nevertheless, the structural trend is described properly by ΔU, i.e., the rigid band concept is useful, at least in the neighborhood of $N=16$ for which the actual DOS were used for deriving the band energies.

V. ELASTIC PROPERTIES

The elastic constants at equilibrium volumes are listed in Tables IV and V for the C15 and C14 structures of $ZrCr_2$. Although C14 is not the stable ground state we discuss its properties because it is a very common structure for Laves phases closely related to $ZrCr_2$, and it might appear at high temperatures.

For the C15 structures of $TiCr_2$ and $ZrCr_2$ we are able to compare our results with calculated data of the NFP approach.[13] For $TiCr_2$ NFP yielded a significantly larger value for c_{11}, the bulk modulus being almost the same which is due to the lower value of c_{12} as shown in Table IV. This stronger anistropy (as compared to our calculation) results in a significantly larger value for c'. Within NFP the LDA was applied (we—in contrast—applied GGA), thus larger values of the elastic constants in general would be expected but not such a strong influence on the anisotropy. For C15 $ZrCr_2$ and $HfCr_2$, it should be noted that the elastic constants calculated by Hong and Fu[14] using FLAPW with LDA are significantly smaller with respect to our present data as well as to the results of Mayer *et al.*[13] This presumably is due to the fact that Hong and Fu derived the elastic constants at the experimental volume which must be significantly larger than the LDA equilibrium volume would be. Even in our case applying a GGA functional our calculated equilibrium volume is smaller by about 3% than the experimental one.

TABLE V. *Ab initio* elastic constants, bulk moduli B, and $c_{66}=(c_{11}-c_{12})/2$ (all in GPa) at the equilibrium volumes for the hexagonal C14 structure of $TiCr_2$, $ZrCr_2$, and $HfCr_2$. The values for (B) are derived from volume derivatives of the total energies.

	c_{11}	c_{12}	c_{13}	c_{33}	c_{44}	c_{66}	B(B)
$TiCr_2$	323	141	150	301	98	91	203 (199)
$ZrCr_2$	272	132	141	246	20	70	180 (176)
$HfCr_2$	302	139	148	275	51	81	194 (191)

The precision of our calculation of the bulk modulus can be estimated by comparing the value directly obtained from the elastic constants, namely $B=(c_{11}+2c_{12})/3$ for cubic and $B=2(c_{11}+c_{12}+2c_{13}+c_{33}/2)/9$ for hexagonal crystals, to the value derived from the volume derivative of the total energy, denoted by (B) in Tables IV and V. In all the cases, the difference is in the range of 2% or smaller. For $ZrCr_2$, the agreement between the two calculational approaches is good. However, the calculated data are about 10% larger than a reported experimental value. Foster *et al.*[28] measured the bulk moduli of the C15 structure of $ZrCr_2$ from 20 to 300 K, indicating a normal temperature dependence showing a decreasing bulk modulus with increasing temperature. The value of 162 GPa in Table IV refers to the measurement at 20 K.

In general, for the C15 as well as for the C14 structure the elastic constants of $TiCr_2$ are largest, the values for $ZrCr_2$ are smallest with $HfCr_2$ in between. This reflects the trend of the energies of formation which is always smallest for all the structures of $ZrCr_2$ shown in Fig. 2. Although—concerning the energies of formation—$HfCr_2$ is very close to $TiCr_2$, its elastic constants are generally smaller than for the Ti compound. Table V shows the 6 elastic constants for the hexagonal C14 structure with a remarkably small value for c_{44} of $ZrCr_2$. Although c_{44} is unusually small, no elastic instability follows from that. On the other hand, this small value results in exceptionally small anisotropy parameters of 0.34 for $A2=(4c_{44})/(c_{11}+c_{33}-2c_{13})$ (referring to $<110]$ slips), and 0.28 for $A3=c_{44}/c_{66}$ (referring to shears in the {100} planes). As a comparison, the values for $TiCr_2$ are 1.2 and 1.1, for $HfCr_2$ 0.61 and 0.66 for A2 and A3, respectively.

From the single crystal elastic constants we derived polycrystalline averages according to Hill,[40] such as Young's modulus E and shear modulus G, Poisson's ratio ν, and elastic anisotropy A as presented in Table VI for the C15 structure, and Table VII for the C14 structure. The polycrystalline averages were obtained for random orientations of the crystallites. Again, Tables VI and VII indicate that all the elastic moduli of $ZrCr_2$ are smallest in accordance to the trend discussed above. Concerning $TiCr_2$ with C14 structure, the experimental values for E and G are smaller with respect to the *ab initio* calculations (Table VII), whereas for $ZrCr_2$ with C15 structure the values for E and G are substantially larger (Table VI). It should be noted that the experiments for the C14 structure of $TiCr_2$ were performed at 1273 K;[26] the *ab initio* elastic constants, however, refer to very low temperatures.

Important materials parameters such as the average sound velocities v_m and Debye temperatures Θ_D were derived as

TABLE VI. Young's moduli E, shear moduli G (all in GPa), Poisson's ratio ν, and elastic anisotropy A according to the average of Hill for the cubic polycrystalline C15 structure of $TiCr_2$, $ZrCr_2$, and $HfCr_2$.

	E	G	ν	A	Ref.
$TiCr_2$	200	75	0.336	1.19	VASP
	248	96	0.30		NFP[a]
$ZrCr_2$	146	54	0.366	1.02	VASP
	156	58	0.36		NFP[a]
	173	66	0.322		Expt.[b]
$HfCr_2$	176	65	0.349	1.007	VASP

[a]Reference 13.
[b]Reference 28.

shown in Table VIII. For $TiCr_2$ the largest B and G values and the smallest molecular weight result in the largest sound velocity and Debye temperatures compared to $ZrCr_2$ and $HfCr_2$. Concerning the C15 structure, Θ_D is now larger for $ZrCr_2$ than for $HfCr_2$ which is a consequence of the larger value of v_m for the Zr compound.

VI. VIBRATIONAL PROPERTIES

Figure 5 shows the phonon dispersion relations and the density of states (DOS) for $ZrCr_2$ calculated at the equilibrium volumes of the C14 and C15 structures. There are 18 (for C15) and 36 (for C14) phonon branches due the number of atoms in the unit cell (6 and 12 for C15 and C14, respectively). Because of the higher symmetry, the features of the DOS for the C15 structure are much sharper. A further significant difference between the dispersions of the two structures is seen in the frequency range between 2 and 3.5 THz. There, no modes exist for the C15 structure in contrast to C14 for which highly dispersive bands are seen in particular around the point A, and close to A a soft mode arises. However, these extra bands of the C14 structure have no visible influence on the DOS due to their steep dispersion. The decomposition of the phonon DOS shows that the broad peak structure centered around 4.5 THz is due to a mixture of Zr- and Cr-like modes for both structures. The peak centered at 7 THz is of rather pure Cr character which is of (6*h*) type in the C14 case. At 6 THz the C15 DOS shows a deep minimum which in the C14 is a rather broad structure. Vibrations

TABLE VII. Young's moduli E, shear moduli G (all in GPa), Poisson's ratio ν, and elastic anisotropy A according to the average of Hill for the hexagonal polycrystalline C14 structure of $TiCr_2$, $ZrCr_2$, and $HfCr_2$.

	E	G	ν	Ref.
$TiCr_2$	240	92	0.303	VASP
	184	71	0.31	Expt.[a]
$ZrCr_2$	91	32	0.415	VASP
$HfCr_2$	161	59	0.362	VASP

[a]Reference 26.

TABLE VIII. Average sound velocities v_m (ms^{-1}) and Debye temperatures Θ_D (K) at calculated equilibrium volumes.

	C15		C14	
	v_m	Θ_D	v_m	Θ_D
$TiCr_2$	3634.6	451.9	4388.2	541.2
$ZrCr_2$	2893.5	345.0	2447.3	291.6
$HfCr_2$	2620.1	315.4	2708.5	324.8

above 8 THz are exclusively of Cr character, because its atomic mass is lighter than the mass of Zr.

From the phonon DOS the phonon free energy F_{ph} can be derived from the equations

$$F_{\mathrm{ph}}(T) = U_{\mathrm{ph}}(T) - TS_{\mathrm{ph}}(T) \tag{3}$$

by defining the phonon free enthalpy

$$U_{\mathrm{ph}}(T) = \frac{1}{2}\int_0^\infty g(\omega)\hbar\omega \coth\left(\frac{\hbar\omega}{2k_BT}\right)d\omega \tag{4}$$

and phonon entropy

$$S_{\mathrm{ph}}(T) = k_B\int_0^\infty g(\omega)\left(\frac{\hbar\omega}{2k_BT}\left[\coth\left(\frac{\hbar\omega}{2k_BT}\right) - 1\right] - \ln\left[1 - \exp\left(-\frac{\hbar\omega}{k_BT}\right)\right]\right)d\omega, \tag{5}$$

where $g(\omega)$ represents the phonon DOS as a function of fre-

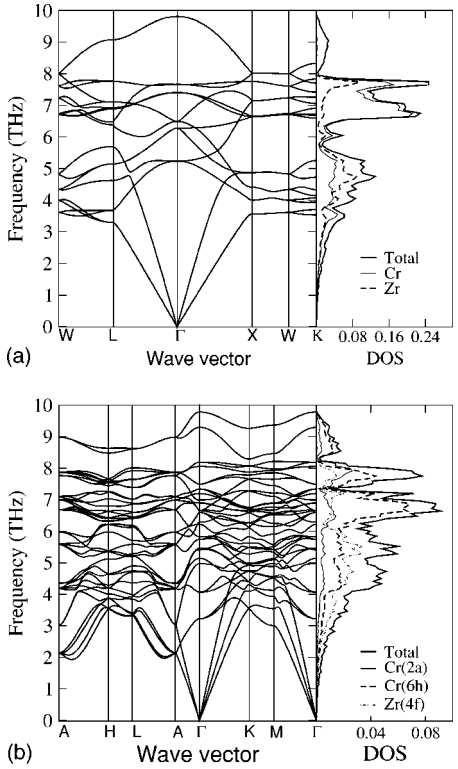

FIG. 5. *Ab initio* phonon dispersion relations and density of states for $ZrCr_2$ in the C15 (upper panel) and C14 (lower panel) structure.

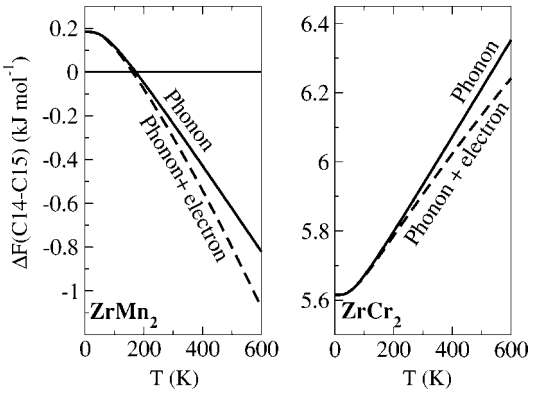

FIG. 6. Differences of total free energies $\Delta F = F_{C14} - F_{C15}$. Results with (solid line) and without (dashed) temperature dependent electronic contributions (Ref. 41). Left panel: $ZrMn_2$; right panel: $ZrCr_2$. Positive values: C15 is stable structure; negative values: C14 is stable structure.

quency ω. In our calculation the total free energy is defined by the relation $F(T) = F_{el}(T) + F_{ph}(T)$ in which the electronic contribution $F_{el}(T) = U_{DFT} + F_{gas}(T)$ consists of the total energy derived from the DFT calculation U_{DFT} and a temperature dependent term $F_{gas}(T)$ coming from the free electron gas model according to the Sommerfeld expansion.[41]

The difference of total free energies $\Delta F = F_{C14} - F_{C15}$ corresponding to the C14 and C15 structures of $ZrCr_2$ and $ZrMn_2$ are shown in Fig. 6. The energy scales in the two panels are different because of the very different structural energies: for $ZrCr_2$ the energy U_{DFT} for the C15 structure is much lower than for C14 whereas for $ZrMn_2$ the corresponding energies are close to be degenerate. Furthermore, the temperature dependence of the structural free energy difference for $ZrMn_2$ is totally opposite to $ZrCr_2$. Although for $ZrMn_2$ at very low temperatures C15 is stable the C14 structure is stabilized above a transition temperature of 160 K due to the phonon free energy difference.[9] The structural stability of $ZrCr_2$ is quite different: at very low temperature C15 is already much more stable than is the case for the Mn compound. With increasing temperature, C15 gains even more which corresponds to the experimental findings: C15 is stable up to rather high temperatures of more than 1800 K at which hexagonal structures appear.[44] These temperatures are far too high to justify any statement on the basis of the harmonic model inherent to the derivation of the phonon DOS and free energy.

In Fig. 7 the phonon free energy differences ΔF_{ph} are decomposed into the the enthalpy contributions ΔU_{ph} and the entropy terms $-T\Delta S_{ph}$. In both cases, for $ZrMn_2$ as well as for $ZrCr_2$, the temperature dependence of both quantities is just opposite. However, noting the scale in the figures the entropies are by far the dominant contributions to the structural free energy difference of the phonons.

In the case of $ZrCr_2$ the zero point energies are very similar amounting to 10.6 for the C15 structure and 10.7 kJ mol^{-1} for the C14 structure.

Figure 8 shows the specific heat for the C14 and C15 structures of $ZrCr_2$. Whereas for the full phonon calculation the curves nearly coincide, for the results based on the Debye

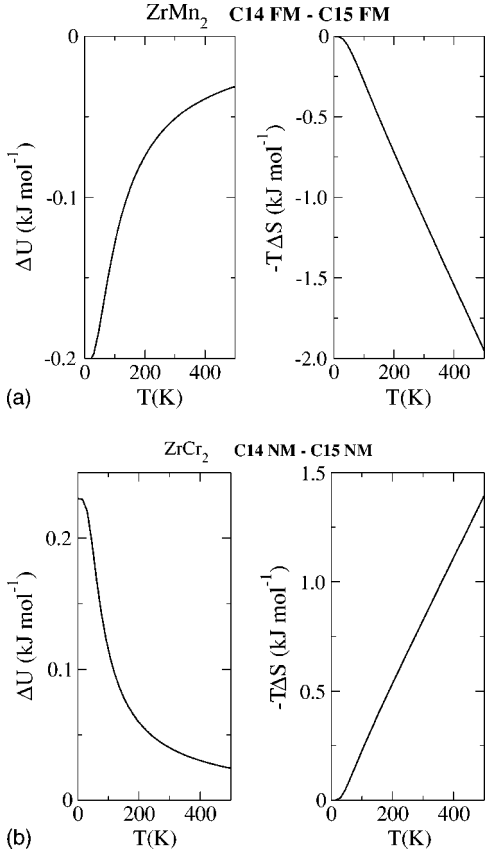

FIG. 7. Upper panels: Phonon enthalpy ΔU_{ph} and entropy $-T\Delta S_{ph}$ decomposition of the structural phonon free energy difference for $ZrMn_2$. Lower panels: Same decomposition for $ZrCr_2$.

approximation (Debye temperatures from Table VIII are applied) a significant splitting between C14 and C15 is observed with all the Debye results being larger than the full phonon results. The largest differences occur at about 200 K.

VII. POINT DEFECTS

For $ZrCr_2$ we studied the formation energies and related quantities for point defects such as vacancies V(Zr) at the Zr and V(Cr) at the Cr sites, and antisite defects Zr^{Cr} for Zr

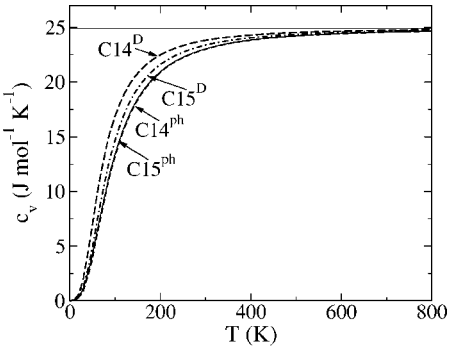

FIG. 8. Lattice specific heat for C14 and C15 structures of $ZrCr_2$. Full phonon calculation denoted by ph; Debye results marked by *D*.

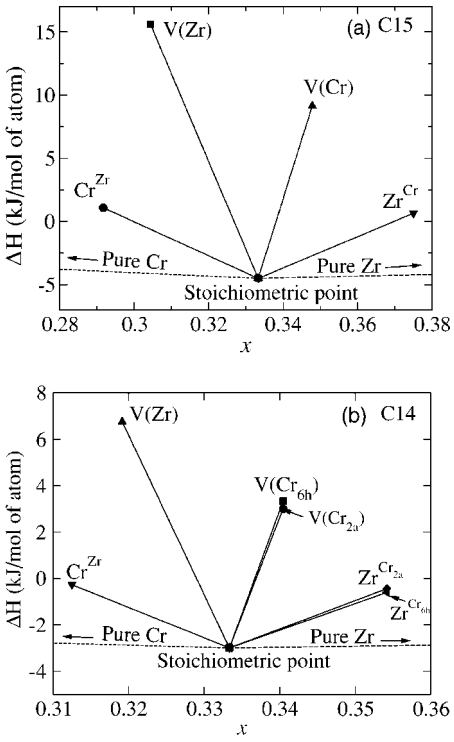

FIG. 9. *Ab initio* enthalpies of formation for compounds Zr_xCr_{1-x} corresponding to the defect supercells versus the concentration x of Zr atoms for the C15 structure (upper panel) and the C14 structure (lower panel). V(Zr): vacancy at Zr site, V(Cr): vacancy at Cr ($2a$) and ($6h$) sites, Zr^{Cr}: Zr at the Cr ($2a$) and ($6h$) sites, Cr^{Zr}: Cr at Zr site.

occupying a Cr site and Cr^{Zr} for the reversed occupation. In the C15 structure because of symmetry there are only four possible arrangements. However, for the C14 structure the Cr atoms occupy the geometrically different ($2a$) and ($6h$) sites which results in six different defect structures. This can be seen in Fig. 9 which shows the enthalpies of formation per atom for the Zr_xCr_{1-x} compounds corresponding to the constructed supercells. These energies are derived directly from density functional total energies as defined in Eq. (1).

Because there is only one experimentally observed ordered compound with a concentration between pure Cr and pure Zr, namely the Laves phase $ZrCr_2$, the two dashed lines marking the boundaries of thermodynamical stability in Fig. 9 are connecting the value for $ZrCr_2$ with zero for the concentrations $x=0$ and 1. It is obvious that the antisite defects are much closer to stability and will therefore dominate. Furthermore, by comparison of the two panels (note the different energy scales) it is also clear that defects (in particular vacancies) in the C15 compound will be more costly in terms of energy.

TABLE IX. Defect formation energies for the C14 and C15 structure for the stoichiometric composition corresponding to $ZrCr_2$ at 1000 K as derived from a statistical mechanic model (see text).

	V(Zr)	V(Cr)	Zr^{Cr}	Cr^{Zr}	
C15	4.77	3.34	1.39	1.39	present work
C15	4.77	3.61	1.23	1.17	Krčmar and Fu[a]
C14	4.65	2.86	1.21	1.21	present work

[a]Reference 15.

The discussed energies are derived with respect to the pure bcc-Cr and hcp-Zr phases. A certainly more realistic description of defects is based on the ordered compound $ZrCr_2$ as a reference and suitable chemical potentials describing the variation of stoichiometry within a grand canonical formulation of a statistic mechanical model.[42] Then, temperature and concentration dependent defect formation energies and concentrations can be derived. Due to the selected supercells and the corresponding concentration variation (i.e., the validity limit of the chemical potentials for each atomic species) the derived results are meaningful in a concentration range of about 2% around the stoichiometric $x=\frac{1}{3}$ composition. In the statistical model the defects are assumed to be independent and they are only linked together by the requirement of conserving a given stoichiometry. For the C14 structure we also make no distinction between defects at Cr ($2a$) or ($6h$) sites because their energies are practically the same according to Fig. 9.

By application of the statistic mechanical model the results given in Tables IX and X were derived. Table IX lists the thermodynamically defined defect formation energies which clearly demonstrate the order of stability for the types of defects as discussed for the supercells. The most costly defect is a vacancy at the Zr site rather independent of the structure. Vacancies at Cr sites would be more favorable by 0.5 eV for the C14 structure for which also the antisite energy is slightly more favorable. The comparison of our data for the C15 structure to the calculation of Ref. 15 shows a significant difference for the vacancy at the Cr site and also for the antisite energy. This difference has possibly two ori-

TABLE X. Calculated temperature dependence of defect concentrations for the C14 and C15 structure for the stoichiometric composition corresponding to $ZrCr_2$.

	C15			C14		
T(K)	V(Cr)	V(Zr)	anti	V(Cr)	V(Zr)	anti
500	2.28E-37	8.99E-48	1.05E-14	1.38E-29	1.25E-47	6.37E-13
1000	1.51E-17	9.49E-25	1.02E-07	3.72E-15	3.54E-24	7.98E-07
1200	9.61E-15	9.57E-21	1.50E-06	9.44E-13	2.87E-20	8.29E-06
1400	9.66E-13	6.93E-18	1.02E-05	4.93E-11	1.78E-17	4.41E-05
1600	3.06E-11	9.68E-16	4.28E-05	9.60E-10	2.22E-15	1.51E-04

gins: in Ref. 15 the lattice parameter was fixed to the experimental value whereas in our case the optimized lattice parameters of the defect-free $ZrCr_2$ compound was taken. Furthermore, the antisite formation energies presented in Ref. 15 are nonequal at the stoichiometric composition, differently to our results. They should, however, be equal for systems of the antistructure type like $ZrCr_2$ because the defect model of Mishin and Herzig[43] as applied in Ref. 15 is very similar to our approach.[42]

The strongly dominant defects are the antisites as revealed by their concentration as a function of temperature in Table X. It should, however, be noted that effective defect entropies can lead to a change of the dominating formation mechanism at elevated temperatures as mentioned in the second reference of Ref. 42. The vacancy concentrations are smaller by a factor $\approx 10^{-6}$ for both structures. From experiments[44] it was concluded that also vacancies might contribute to the defect mechanism which is not confirmed by our calculations. However, in this paper it was also stated that the occurrence of certain defect types might depend on the preparation and heat treatment of the samples. The C14 structure is significantly more proned to antisite defects, e.g. by a factor of about 3 when compared to the C15 structure at 1600 K. Because the vacancy formation energies are much larger and the symmetric mixture of antisites is predominant the phase stability region will be rather narrow around the stoichiometric concentration in agreement to the experimental phase diagram.[11] This situation is very different for $ZrMn_2$ for which the easy formation of Mn antisites produces a broad stoichiometry range towards the Mn rich side of the 1:2 composition.

VIII. SUMMARY AND CONCLUSION

By application of the DFT approach VASP the structural stabilities, heats of formation, electronic structures and elastic properties have been investigated for the Cr-based isoelectronic Laves phases $TiCr_2$, $ZrCr_2$, and $HfCr_2$ with the cubic C15 and hexagonal C14 and C36 crystal structures. The experimental finding of very stable C15 phases is quantitatively confirmed and the trend of structural stability when varying the number of valence electrons is discussed in terms of band energies. The comparison with the few existing reliable experimental data shows rather good agreement proving the validity of the *ab initio* approach. In addition, for the C14 and C15 structures of $ZrCr_2$, phonon dispersions, temperature dependent free energies, specific heats, and defect properties have been derived from DFT calculations. The results for $ZrCr_2$, in particular structural stabilities, electronic structures, and temperature dependent free energies, are compared to the calculated data for $ZrMn_2$ which has unusual properties as published recently.[9]

ACKNOWLEDGMENTS

The study was supported by the Austrian Science Fund FWF Project No. P16957. Most of the calculations were performed on the Schrödinger-2 PC cluster of the University of Vienna. X.Q.C. is grateful to the OEAD for support within the Austrian Chinese technical scientific exchange program, Project No. VII.A.16.

[1] A. von Keitz and G. Sauthoff, Intermetallics **10**, 497 (2002).
[2] I. Jacob and D. Shaltiel, J. Less-Common Met. **65**, 117 (1979).
[3] S. Kuranaka, T. Gamo, and Y. Morita, J. Alloys Compd. **253-254**, 268 (1997); V. V. Pet'kov, S. B. Prima, L. A. Fret'jacenko, and Ju. A. Kocerzhinsrij, Metallofizika (Kiev) (Akademiya Nauk Ukrainskoi SSR, Institut Metallofiziki) **46**, 80 (1973).
[4] P. M. Hazzledine and P. Pirouz, Scr. Metall. Mater. **28**, 1277 (1993).
[5] F. R. de Boer, R. Boom, W. C. M. Mattens, A. R. Miedema, and A. K. Nissen, in *Cohesion in Metals: Transition Metal Alloys*, edited by F. R. de Boer and D. G. Pettifor (North-Holland, Amsterdam, 1989), Vol. 1.
[6] O. Kubaschewski, C. B. Alcock, and P. J. Spencer, *Materials Thermochemistry*, 6th ed. (Pergamon, Oxford, 1993).
[7] F. Laves, *Theory of Alloy Phases* (American Society for Metals, Metals Park, OH, 1956), p. 124.
[8] T. B. Massalski, in *Intermetallic Compounds*, edited by J. H. Westbrook (Wiley, New York, 1967), p. 197.
[9] X. Q. Chen, W. Wolf, R. Podloucky, P. Rogl, and M. Marsman, Europhys. Lett. **67**, 807 (2004).
[10] X. Q. Chen, W. Wolf, R. Podloucky, P. Rogl, and M. Marsman (to be published).
[11] T. B. Massalski, J. L. Murray, L. H. Bennett, and H. Baker, in *Binary Alloy Phase Diagram* (American Society for Metals, Metals Park, OH, 1986).
[12] H. Anton and P. C. Schmidt, Intermetallics **5**, 449 (1997).
[13] B. Mayer, H. Anton, E. Bott, M. Methfessel, J. Sticht, J. Harris, and P. C. Schmidt, Intermetallics **11**, 23 (2003).
[14] S. Hong and C. L. Fu, Intermetallics **9**, 799 (2001).
[15] M. Krčmar and C. L. Fu, Phys. Rev. B **68**, 134110 (2003).
[16] G. Kresse and J. Hafner, Phys. Rev. B **48**, 13 115 (1993); G. Kresse and J. Furthmüller, Comput. Mater. Sci. **6**, 15 (1996); Phys. Rev. B **54**, 11 169 (1996).
[17] P. E. Blöchl, Phys. Rev. B **50**, 17 953 (1994).
[18] G. Kresse and D. Joubert, Phys. Rev. B **59**, 1758 (1999).
[19] J. P. Perdéw and Y. Wang, Phys. Rev. B **45**, 13 244 (1992).
[20] H. J. Monkhorst and J. D. Pack, Phys. Rev. B **13**, 5188 (1976).
[21] K. Parlinski, Software Phonon 3.11 (2002) as implemented in MedeA, Materials Design s.a.r.l. (2003), www.materialsdesign.com; K. Parlinski, Z.-Q. Li, and Y. Kawazoe, Phys. Rev. Lett. **78**, 4063 (1997); G. Kresse, J. Furthmüller, and J. Hafner, Europhys. Lett. **32**, 729 (1995).
[22] B. Meyer, V. Schott, and M. Fähnle, Phys. Rev. B **58**, R14673 (1998).
[23] F. B. Cuff, N. J. Grant, and C. F. Floe, Trans. AIME **194**, 848 (1952); V. N. Svechnikov, M. Yu. Teslyuk, Yu. A. Kocherzhinsky, V. V. Petkov, and E. V. Dabizha, Dopov. Akad. Nauk Ukr. RSR, Ser. A: Fiz.-Tekh. Mat. Nauki **9**, 837 (1970).
[24] J. F. Lynch, J. R. Johnson, and R. C. Bowman, NATO Conf. Ser. **6**, 437 (1983); R. P. Elliott and W. Rostocker, Trans. Am. Soc.

Met. **50**, 617 (1958).
[25] V. Ya. Markiv and V. V. Burnashova, Sov. Powder Metall. Met. Ceram, translated from Poroshkdvaya metallurgiya, Kiev, **9**, 998 (1970).
[26] R. L. Fleischer, R. S. Gilmore, and R. J. Zabala, J. Appl. Phys. **64**, 2964 (1988).
[27] J. L. Soubeyroux, M. Bououdina, D. Fruchart, and P. de Range, J. Alloys Compd. **231**, 760 (1995); J. L. Soubeyroux, M. Bououdina, D. Fruchart, and L. Pontonnier, *ibid.* **219**, 48 (1995).
[28] K. Foster, J. E. Hightower, R. G. Leisure, and A. V. Skripov, Philos. Mag. B **80**, 1667 (2000).
[29] S. A. Minayeva and P. B. Budberg, Russ. Metall. **3**, 179 (1975).
[30] R. P. Elliott, Trans. Am. Soc. Met. **53**, 321 (1961).
[31] S. A. Minayeva, P. B. Buderg, and E. A. Shishkin, Metallofizika (Kiev) (Akademiya nauk ukrainskoi SSR, Institut Metallofiziki), **52**, 98 (1974).
[32] X. Q. Chen, V. T. Witusiewicz, R. Podloucky, P. Rogl, and F. Sommer, Acta Mater. **51**, 1239 (2003).
[33] X. Q. Chen, W. Wolf, R. Podloucky, and P. Rogl, Intermetallics **12**, 59 (2004).
[34] G. Cacciamani, P. Riani, G. Borzone, N. Parodi, A. Saccone, R. Ferro, A. Pisch, and R. Schmid-Fetzer, Intermetallics **7**, 101 (1999).
[35] I. N. Pyagai and A. V. Vakhobov, Russ. Metall. **5**, 50 (1990).
[36] Q. Guo and O. J. Kleppa, J. Alloys Compd. **269**, 181 (1998).
[37] Q. Guo and O. J. Kleppa, J. Alloys Compd. **266**, 224 (1998).
[38] A. V. Skripov and A. V. Mirmelstein, J. Phys.: Condens. Matter **5**, L619 (1993); A. V. Skripov, A. E. Karkin, and A. V. Mirmelstein, *ibid.* **9**, 1191 (1997).
[39] D. A. Pankhurst, D. Nguyen-Manh, and D. G. Pettifor, Phys. Rev. B **69**, 075113 (2004).
[40] M. Nakamura, in *Basic Mechanical Properties and Lattice Defects of Intermetallic Compounds*, edited by J. H. Westbrook and R. L. Fleischer (Wiley, New York, 1995), p. 1.
[41] W. Ashcroft and N. D. Mermin, *Solid State Physics* (Holt, Rinehart and Winston, New York, 1976), p. 47.
[42] B. Meyer and M. Fähnle, Phys. Rev. B **59**, 6072 (1999); **60**, 717 (1999); M. Rasamny, M. Weinert, G. W. Fernando, and R. E. Watson, *ibid.* **64**, 144107 (2001).
[43] Y. Mishin and Chr. Herzig, Acta Mater. **48**, 589 (2000).
[44] S. Kanazawa, Y. Kaneno, H. Inoue, W. Y. Kim, and T. Takasugi, Intermetallics **10**, 783 (2002).